Embedded WENO : a design method to improve existing WENO schemes

EINDHOVEN UNIVERSITY OF TECHNOLOGY
Department of Mathematics and Computer Science

CASA-Report 15-29
July 2015

Embedded WENO: a design method to improve existing WENO schemes

by

B.S. van Lith, J.H.M. ten Thije Boonkkamp, W.L. IJzerman

Centre for Analysis, Scientific computing and Applications
Department of Mathematics and Computer Science
Eindhoven University of Technology
P.O. Box 513
5600 MB Eindhoven, The Netherlands
ISSN: 0926-4507

Embedded WENO: a design method to improve existing WENO schemes

Bart S. van Lith[a,1], Jan H.M. ten Thije Boonkkamp[a], Wilbert L. IJzerman[b]

[a]*Department of Mathematics and Computer Science, Eindhoven University of Technology - P. O. Box 513, NL-5600 MB Eindhoven, The Netherlands.*
[b]*Philips Lighting.*

Abstract

Embedded WENO methods utilize all adjacent smooth substencils to construct a desirable interpolation. Conventional WENO schemes underuse this possibility close to large gradients or discontinuities. Embedded methods based on the WENO schemes of Jiang and Shu [1] and on the WENO-Z scheme of Borges et al. [2] are explicitly constructed. Several possible choices are presented that result in either better spectral properties or a higher order of convergence. The embedded methods are demonstrated to be improvements over their standard counterparts by several numerical examples. All the embedded methods presented have virtually no added computational effort compared to their standard counterparts.

Keywords: Essentially non-oscillatory, WENO, high-resolution scheme, hyperbolic conservation laws, nonlinear interpolation, spectral analysis.

In a seminal paper in 1987, Harten and Osher introduced the essentially non-oscillatory (ENO) reconstruction technique [3]. The basic idea of ENO is to construct several different candidate polynomial interpolations and to choose the smoothest approximation to work with. The choice is facilitated by means of smoothness indicators, which become larger as the interpolation varies more rapidly.

Building on the ENO scheme, Liu, Osher and Chan introduced the weighted essentially non-oscillatory (WENO) reconstruction technique in 1994 [4]. The

Email address: b.s.v.lith@tue.nl (Bart S. van Lith)
[1]Corresponding author

WENO technique comes from the realization that the three approximations of ENO can be combined to construct a higher-order approximation. Instead of the logical statements inherent in the ENO scheme, the WENO scheme weighs every lower-order approximation according to its smoothness indicator. Thus, in smooth regions, WENO gives a better approximation, while reducing to ENO near discontinuities.

WENO schemes are ubiquitous in science and engineering, with applications in fluid dynamics, astrophysics, or any other application involving convection-dominated dynamics [5, 6]. The technique is mainly applied in the context of hyperbolic and convection-dominated parabolic PDEs. However, since it is a highly advanced interpolation technique, it also has applications in fields that do not use it as part of a PDE solver, such as computer vision and image processing [7, 8].

The standard WENO scheme as it is most commonly used today was devised by Jiang and Shu [1], and is sometimes referred to as the WENO-JS scheme. Recently, several variants of the WENO scheme have appeared that improve the order of accuracy near points where the first derivative vanishes. Several examples include the WENO-M [9, 10], WENO-Z [2, 11, 12] and WENO-NS [13] schemes. For a comparison of the performance of these schemes, see Zhao et al. [14]. Other efforts have focussed on creating energy-stable WENO schemes such as those constructed by Yamaleev et al. [15, 16].

The most common implementations of WENO schemes use a five-point stencil, which can be subdivided into three three-point stencils. WENO schemes switch seamlessly between the third and fifth-order reconstructions that are possible on the five-point stencil. The idea is straightforward: when all three smoothness indicators are roughly equal, a WENO scheme switches to the fifth-order mode. When one or more smoothness indicators are large, a WENO scheme switches to the third-order mode.

In this formulation, it seems obvious that information is discarded when only one out of three smoothness indicators is large. When this happens, the two smooth approximations could still be used to obtain better accuracy. The current WENO methods do not allow for control over the numerical solution in this situation. In this work, we propose a method that does exactly this. Moreover, we shall explicitly construct two variants of the WENO scheme that exhibit this property.

Apart from the order of convergence, one can also analyse a WENO scheme in terms of its spectral properties [17]. WENO schemes switch non-linearly between linear modes of operation and as such, it is possible to

investigate the spectral properties by analysing the underlying linear schemes [18]. We will also show that our method allows for the tuning of spectral properties such as dispersion and dissipation.

This paper is arranged in the following way: in Section 1 we give a short recap of WENO methods, in Section 2 we introduce the embedding method, in Section 3 we look at the spectral properties of the embedded schemes and in Section 4 we show results of several numerical experiments. Finally, we present our conclusions and outlook in Section 5.

1. The classical WENO scheme

The WENO method is an advanced interpolation technique that aims to suppress spurious oscillations. It is commonly used in as part of a high-resolution scheme for hyperbolic conservation laws, e.g.,

$$\frac{\partial u}{\partial t} + \frac{\partial}{\partial x} f(u) = 0, \tag{1}$$

where f is the flux function. To obtain numerical solutions, we introduce a grid, $\{x_j\}_{j=1}^{N}$, with grid size Δx. With each point x_j, we associate a cell centred on x_j of width Δx, i.e., the interval $(x_{j-\frac{1}{2}}, x_{j+\frac{1}{2}})$. Taking the average of the conservation law over cell j, we find

$$\frac{\mathrm{d}u_j}{\mathrm{d}t} + \frac{1}{\Delta x}\left(f(u(x_{j+\frac{1}{2}}, t)) - f(u(x_{j-\frac{1}{2}}, t))\right) = 0, \tag{2}$$

where u_j is the average value of u over cell j. Note that this ODE for the average value u_j is exact as long as we know the exact value of u on the cell boundaries. We shall, in the following, suppress the explicit time dependence of u, as we interpolate u in space for fixed time. In a numerical scheme, we introduce a numerical flux function to represent the fluxes on the cell edges. Regardless of the choice of numerical flux, we require the value of u at the cell interfaces $x_{j\pm\frac{1}{2}}$, i.e. $u(x_{j\pm\frac{1}{2}})$. However, if u is discontinuous and we would naively use polynomial interpolation, we inadvertently introduce spurious oscillations. A (W)ENO scheme is a more advanced interpolation technique that is designed to suppress these oscillations.

The classical WENO scheme, or WENO-JS, can be constructed by considering a five-point stencil around x_j, i.e., $S = \{x_{j-2}, x_{j-1}, x_j, x_{j+1}, x_{j+2}\}$. The large stencil can be divided into three smaller substencils, viz., $S_0 =$

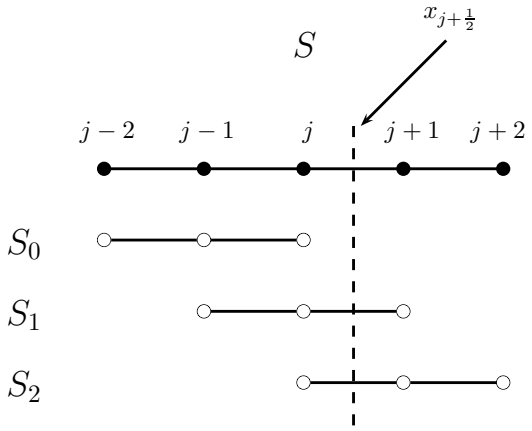

Figure 1: The five-point stencil S, with substencils S_0, S_1 and S_2. Note that the stencil is asymmetric around the interpolation point.

$\{x_{j-2}, x_{j-1}, x_j\}$, $S_1 = \{x_{j-1}, x_j, x_{j+1}\}$ and $S_2 = \{x_j, x_{j+1}, x_{j+2}\}$; see Figure 1.

On each of these substencils, we can construct a second-degree polynomial p_k that has the same cell averaged values as u, i.e.,

$$\frac{1}{\Delta x} \int_{x_{j-\frac{1}{2}}}^{x_{j+\frac{1}{2}}} p_k(x)\,\mathrm{d}x = u_j. \tag{3}$$

Evaluating these polynomials on the cell edge $x_{j+\frac{1}{2}}$, we obtain three approximations for $u(x_{j+\frac{1}{2}})$, given by

$$u^{(0)}_{j+\frac{1}{2}} = \tfrac{1}{6}(2u_{j-2} - 7u_{j-1} + 11u_j), \tag{4a}$$

$$u^{(1)}_{j+\frac{1}{2}} = \tfrac{1}{6}(-u_{j-1} + 5u_j + 2u_{j+1}), \tag{4b}$$

$$u^{(2)}_{j+\frac{1}{2}} = \tfrac{1}{6}(2u_j + 5u_{j+1} - u_{j+2}). \tag{4c}$$

Note that approximation $u^{(k)}_{j+\frac{1}{2}}$ takes only information from S_k for $k = 0, 1, 2$. These approximations are third-order accurate, and their errors are given by

$$u^{(0)}_{j+\frac{1}{2}} - u(x_{j+\frac{1}{2}}) = -\tfrac{1}{4}\Delta x^3 \partial_x^3 u(x_{j+\frac{1}{2}}) + \tfrac{3}{10}\Delta x^4 \partial_x^4 u(x_{j+\frac{1}{2}}) + \mathcal{O}(\Delta x^5), \quad (5a)$$

$$u^{(1)}_{j+\frac{1}{2}} - u(x_{j+\frac{1}{2}}) = \tfrac{1}{12}\Delta x^3 \partial_x^3 u(x_{j+\frac{1}{2}}) - \tfrac{1}{30}\Delta x^4 \partial_x^4 u(x_{j+\frac{1}{2}}) + \mathcal{O}(\Delta x^5), \quad (5b)$$

$$u^{(2)}_{j+\frac{1}{2}} - u(x_{j+\frac{1}{2}}) = -\tfrac{1}{12}\Delta x^3 \partial_x^3 u(x_{j+\frac{1}{2}}) - \tfrac{1}{30}\Delta x^4 \partial_x^4 u(x_{j+\frac{1}{2}}) + \mathcal{O}(\Delta x^5). \quad (5c)$$

It is straightforward to show that one can obtain a fifth-order approximation by taking a linear combination of the third-order approximations of (4). The coefficients are the unique numbers that sum to unity and eliminate the third and fourth-order error of the Taylor expansions in (5). Some linear algebra quickly reveals that we should use

$$u_{j+\frac{1}{2}} = \tfrac{1}{10} u^{(0)}_{j+\frac{1}{2}} + \tfrac{6}{10} u^{(1)}_{j+\frac{1}{2}} + \tfrac{3}{10} u^{(2)}_{j+\frac{1}{2}}. \quad (6)$$

In terms of the cell averages, this fifth-order approximation is given by

$$u_{j+\frac{1}{2}} = \tfrac{1}{60}(2u_{j-2} - 13u_{j-1} + 47u_j + 27u_{j+1} - 3u_{j+2}). \quad (7)$$

Using (5), we find that the error term for this expression is indeed fifth-order, i.e.,

$$u_{j+\frac{1}{2}} - u(x_{j+\frac{1}{2}}) = -\tfrac{1}{60}\Delta x^5 \partial_x^5 u(x_{j+\frac{1}{2}}) + \mathcal{O}(\Delta x^6). \quad (8)$$

The coefficients of (6) are referred to as the linear or optimal weights. We denote the linear weights by $\gamma_0 = \frac{1}{10}$, $\gamma_1 = \frac{6}{10}$ and $\gamma_2 = \frac{3}{10}$.

So far, we have shown that a fifth-order linear approximation can be constructed from three third-order underlying approximations. However, whenever there is a discontinuity on the stencil, the fifth-order approximation incurs spurious oscillations and a third-order approximation might actually be better in some sense. Thus, we would like to find a set of nonlinear weights that takes into account the smoothness of each third-order approximation. Whenever u is smooth on the full stencil S, we want these nonlinear weights to approximate the linear weights. On the other hand, when a substencil contains a discontinuity, we would like to have the weight associated with that stencil to be small.

This idea can be realized by introducing smoothness indicators β_k, $k = 0, 1, 2$. There are several smoothness indicators available in the literature [19, 20], each one exhibiting some desirable property. A very popular set of

indicators, however, were introduced by Jiang and Shu and are given by

$$\beta_k := \int_{x_{j-\frac{1}{2}}}^{x_{j+\frac{1}{2}}} \left(p_k''(x)\right)^2 \Delta x^3 + \left(p_k'(x)\right)^2 \Delta x \, \mathrm{d}x. \tag{9}$$

A tedious but straightforward calculus exercise shows that

$$\beta_0 = \frac{13}{12}(u_{j-2} - 2u_{j-1} + u_j)^2 + \frac{1}{4}(u_{j-2} - 4u_{j-1} + 3u_j)^2, \tag{10a}$$

$$\beta_1 = \frac{13}{12}(u_{j-1} - 2u_j + u_{j+1})^2 + \frac{1}{4}(u_{j-1} - u_{j+1})^2, \tag{10b}$$

$$\beta_2 = \frac{13}{12}(u_j - 2u_{j+1} + u_{j+2})^2 + \frac{1}{4}(3u_j - 4u_{j+1} + u_{j+2})^2, \tag{10c}$$

where one can recognise undivided finite differences. Provided that u is sufficiently smooth, a Taylor expansion reveals that $\beta_k = \mathcal{O}(\Delta x^2)$, where the coefficients of the expansion contain various derivatives of u, either squared or multiplied with higher order derivatives, i.e.,

$$\beta_0 = (u_j')^2\Delta x^2 + \left(\tfrac{13}{12}(u_j'')^2 - \tfrac{2}{3}u_j'u_j'''\right)\Delta x^4 - \left(\tfrac{13}{6}u_j''u_j''' - \tfrac{1}{2}u_j'u_j''''\right)\Delta x^5 + \mathcal{O}(\Delta x^6), \tag{11a}$$

$$\beta_1 = (u_j')^2\Delta x^2 + \left(\tfrac{13}{12}(u_j'')^2 + \tfrac{1}{3}u_j'u_j'''\right)\Delta x^4 + \mathcal{O}(\Delta x^6), \tag{11b}$$

$$\beta_2 = (u_j')^2\Delta x^2 + \left(\tfrac{13}{12}(u_j'')^2 - \tfrac{2}{3}u_j'u_j'''\right)\Delta x^4 + \left(\tfrac{13}{6}u_j''u_j''' + \tfrac{1}{2}u_j'u_j''''\right)\Delta x^5 + \mathcal{O}(\Delta x^6), \tag{11c}$$

where u_j' is shorthand for $\partial_x u(x_j)$, etc. Whereas an ENO scheme uses a logical statement to select the interpolation with the lowest smoothness indicator, a WENO scheme proposes to use a convex combination of the third-order interpolations, much like (6). To this end, the nonlinear weights ω_k are introduced, which are functions of the smoothness indicators. Thus, a WENO scheme uses a linear combination of the form

$$u_{j+\frac{1}{2}} = \omega_0 u^{(0)}_{j+\frac{1}{2}} + \omega_1 u^{(1)}_{j+\frac{1}{2}} + \omega_2 u^{(2)}_{j+\frac{1}{2}}. \tag{12}$$

Consistency requires that the nonlinear weights sum to unity. Hence, to construct nonlinear weights that satisfy the requirements discussed earlier, we first compute the unnormalized nonlinear weights as

$$\tilde{\omega}_k = \frac{\gamma_k}{(\beta_k + \varepsilon)^p}, \tag{13}$$

with $\varepsilon > 0$ a small number to avoid division by zero and $p > 0$. Typical values are $\varepsilon = 10^{-6}$ and $p = 2$. The unnormalized weights are subsequently normalised to obtain the nonlinear weights

$$\omega_k = \frac{\tilde{\omega}_k}{\sum_{i=0}^{2} \tilde{\omega}_i}. \tag{14}$$

The WENO-JS scheme gives fifth-order accuracy whenever u is smooth, i.e., $\beta_k = \mathcal{O}(\Delta x^2)$. At the same time, it gives third-order accuracy whenever a substencil contains a discontinuity, since then the corresponding smoothness indicator becomes large. By choosing instead to use only one of the smooth substencils, oscillations are suppressed.

WENO schemes are commonly employed in a method of lines (MOL) approach, were one leaves time continuous while discretising space. This approach then turns a PDE into a large number of coupled ODEs, resulting in a system of equations

$$\frac{\mathrm{d}\mathbf{u}}{\mathrm{d}t} = L(\mathbf{u}), \tag{15}$$

where L is the result of the WENO scheme. After the spatial discretisation, one discretises time by taking time levels $t^n = n\Delta t$, $n = 0, 1, \ldots$. The time integrators of choice are the strong stability preserving Runge-Kutta methods (SSPRK) [21, 22]. These are explicit Runge-Kutta methods that have a high order of accuracy and do not incur spurious oscillations due to time integration. Throughout this paper, we shall use the fairly standard SSPRK(3,3) method, unless explicitly stated otherwise. One time step of the SSPRK(3,3) method is given by

$$\mathbf{u}^{(1)} = \mathbf{u}^n + \Delta t L(\mathbf{u}^n), \tag{16a}$$

$$\mathbf{u}^{(2)} = \tfrac{3}{4}\mathbf{u}^n + \tfrac{1}{4}\mathbf{u}^{(1)} + \tfrac{1}{4}\Delta t L(\mathbf{u}^{(1)}), \tag{16b}$$

$$\mathbf{u}^{n+1} = \tfrac{1}{3}\mathbf{u}^n + \tfrac{2}{3}\mathbf{u}^{(1)} + \tfrac{2}{3}\Delta t L(\mathbf{u}^{(2)}), \tag{16c}$$

where $\mathbf{u}^{(1)}$ and $\mathbf{u}^{(2)}$ are the intermediate stages. This method exhibits the strong stability preserving property and provides a third-order accuracy in time. Moreover, Wang and Rong [23] have shown that this method is linearly stable when coupled to a five-point WENO scheme. We shall use a CFL number of 0.45 throughout whenever we use the SSP(3,3) method. This value is chosen so the error due to time integration will be small compared to

the spatial error, such that we may detect spatial convergence rates greater than third-order.

Alternatively, we will occasionally use the SSPRK(5,4) method developed by Spiteri and Ruuth [24], which has 5 stages and provides fourth-order accuracy. One can furthermore check from Theorem 3.12 in [23], that it is linearly stable when coupled to a five-point WENO scheme. Spiteri and Ruuth found the coefficients numerically from an optimisation problem, hence they are given to 15 decimals in Table 1.

0	0	0	0	0	0
0.39175222700392	0.39175222700392	0	0	0	0
0.58607968896779	0.21766909633821	0.36841059262959	0	0	0
0.47454236302687	0.08269208670900	0.13995850206900	0.25189177424738	0	0
0.93501063100924	0.06796628370320	0.11503469844438	0.20703489864929	0.54497475021237	0
	0.14681187618661	0.24848290924556	0.10425883036650	0.27443890091960	0.22600748319395

Table 1: Butcher tableau of the SSPRK(5,4) method of Spiteri and Ruuth.

Whereas the SSPRK(3,3) time integrator from (16) is stable for CFL coefficients less than 1, the SSPRK(5,4) is stable for CFL coefficients less than 1.5081. As pointed out by Spiteri and Ruuth, this may lead to more efficient schemes in terms of total number of operations. We have chosen a CFL coefficient of 0.45 for the SSPRK(3,3) scheme, so we may, for instance, chose a CFL coefficient three times larger when using the SSPRK(5,4) integrator. This choice results in three times as few times steps. On the other hand, it does require $\frac{5}{3}$ times as many operations per time step. The upshot is a total amount of $\frac{5}{9}$ times the operations for the numerical solution as compared to SSPRK(3,3). Hence, we may obtain a similar result, perhaps even more accurate, with fewer total operations.

2. Embedded WENO

We now pose the question of what happens when two adjacent substencils are smooth and the third one contains a discontinuity. Thus, either S_0 and S_1 are smooth and S_2 is not or, S_1 and S_2 are smooth and S_0 is not. The answer to the question, of course, is that the WENO-JS scheme still provides third-order accuracy while suppressing oscillations. However, the scheme generates a linear combination of the two smooth substencils that is uncontrollable by the user. A conventional WENO scheme does allow the user to specify the resulting linear combination in this situation.

Let us examine the normalised weights, from the definition (13) - (14) we find that

$$\omega_i^{\text{JS}} = \gamma_i \frac{1}{\gamma_0 \left(\frac{\beta_i+\varepsilon}{\beta_0+\varepsilon}\right)^p + \gamma_1 \left(\frac{\beta_i+\varepsilon}{\beta_1+\varepsilon}\right)^p + \gamma_2 \left(\frac{\beta_i+\varepsilon}{\beta_2+\varepsilon}\right)^p}, \tag{17}$$

where we have labelled the weights with a superscript JS to indicate the WENO-JS weights. Assuming u is smooth, $\varepsilon \ll \beta_i$ for $i = 0, 1, 2$ and using (11), we obtain,

$$\left(\frac{\beta_i+\varepsilon}{\beta_j+\varepsilon}\right)^p = 1 + \mathcal{O}(\Delta x^2), \tag{18}$$

which holds whenever $p > 0$. Therefore, we find that

$$\omega_i^{\text{JS}} = \gamma_i + \mathcal{O}(\Delta x^2). \tag{19}$$

When u is discontinuous on a substencil, the first derivative behaves as $\mathcal{O}(\frac{1}{\Delta x})$, since the jump remains constant while the grid size goes to zero. Suppose that the discontinuity is only in substencil S_0, this leads to $\beta_0 = \mathcal{O}(1)$ from (11). Using this information, we find that

$$\left(\frac{\beta_0+\varepsilon}{\beta_j+\varepsilon}\right)^p = \left(\frac{C}{\Delta x^2}\right)^p (1 + \mathcal{O}(\Delta x^2)), \tag{20}$$

where $j = 1, 2$ and again assuming that $\varepsilon \ll \beta_i$, $i = 1, 2$. From (11), we also find that C is related to the ratio of the size of the jump divided by the derivative of the smooth part. Thus, now the normalised weights are given by

$$\begin{aligned}\omega_0^{\text{JS}} &= \frac{\gamma_0}{\gamma_0 + (\gamma_1+\gamma_2)\left(\frac{C}{\Delta x^2}\right)^p (1 + \mathcal{O}(\Delta x^2))} = \frac{\gamma_0}{\gamma_1+\gamma_2}\left(\frac{\Delta x^2}{C}\right)^p \left(1 + \mathcal{O}(\Delta x^2)\right) \\ &= \mathcal{O}(\Delta x^{2p}).\end{aligned} \tag{21}$$

On the other hand, when we look at the middle stencil S_1, we must investigate a ratio

$$\left(\frac{\beta_1+\varepsilon}{\beta_0+\varepsilon}\right)^p = \mathcal{O}(\Delta x^{2p}). \tag{22}$$

Using this in (17), we find

$$\omega_1^{\text{JS}} = \frac{\gamma_1}{\gamma_1 + \gamma_2(1 + \mathcal{O}(\Delta x^2))} = \frac{\gamma_1}{\gamma_1+\gamma_2} + \mathcal{O}(\Delta x^2). \tag{23}$$

Similarly, for ω_2^{JS} we find

$$\omega_2^{\mathrm{JS}} = \frac{\gamma_2}{\gamma_1 + \gamma_2} + \mathcal{O}(\Delta x^2). \tag{24}$$

Note that the result simply is a redistribution of the weights, keeping the same proportions. Ignoring small terms of order $\mathcal{O}(\Delta x^2)$, we find

$$\omega_1^{\mathrm{JS}} : \omega_2^{\mathrm{JS}} = \gamma_1 : \gamma_2 = 2 : 1. \tag{25a}$$

We can perform a similar computation whenever $\beta_2 = \mathcal{O}(1)$, one finds

$$\omega_0^{\mathrm{JS}} : \omega_1^{\mathrm{JS}} = \gamma_0 : \gamma_1 = 1 : 6. \tag{25b}$$

Moreover, any WENO scheme which switches only between third and fifth-order modes exhibits this behaviour. We propose a technique that allows control over the nonlinear weights in the situation when either $\beta_0 = \mathcal{O}(1)$ or $\beta_2 = \mathcal{O}(1)$. We call this new type of scheme an embedded WENO scheme. Similarly to conventional WENO schemes, we demand fifth-order accuracy whenever the numerical solution is smooth on the entire stencil S. Moreover, it should reduce to an ENO scheme when two out of three substencils contain a discontinuity. However, when there is a discontinuity on the full stencil but we have two adjacent smooth substencils, we wish to have control over the nonlinear weights. In fact, we would like to control the resulting linear combination of the two remaining smooth substencils.

Examining Figure 1, we see that if S_2 contains the discontinuity and S_0 and S_1 are smooth, then the discontinuity must lie in the interval (x_{j+1}, x_{j+2}). Consequently, there are four grid points on which we have a smooth function to interpolate. From the two remaining substencils, we can construct a four-point stencil where we can define our inner scheme. When S_0 contains the discontinuity, we have the four-point stencil $S_{1,2} := S_1 \cup S_2$ to use for the inner scheme. When S_2 contains the discontinuity we have $S_{0,1} := S_0 \cup S_1$.

Let us set the question of how to achieve this aside for the moment and first introduce some terminology. We call the overall third-and-fifth-order accurate scheme the outer scheme. The resulting scheme when there are only two adjacent smooth substencils, we call the inner scheme, see Figure 2. For instance, we may use a fourth-order inner scheme in combination with WENO-JS as the outer scheme.

With the terminology in place we can turn to the basic question: how to embed one WENO scheme in another? Thus, we would like the nonlinear

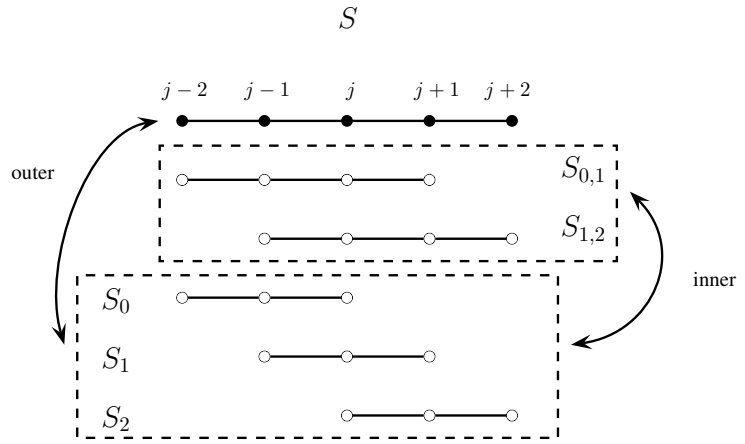

Figure 2: The five-point stencil S, with substencils S_0, S_1 and S_2, and inner scheme stencils $S_{0,1}$ and $S_{1,2}$.

weights to converge to the inner scheme whenever appropriate. Otherwise, they should remain approximately equal to the nonlinear weights of the outer scheme. This suggests that we multiply the unnormalised weights of the outer scheme by a correction that is ordinarily close to unity, but activates when either β_0 or β_2 becomes $\mathcal{O}(1)$. The correction is constructed such that it adjusts the proportions found in (25).

Suppose the inner scheme is given by the linear weights α_0, $\alpha_{0,1}$, $\alpha_{1,2}$ and α_2, such that

$$u^{(0,1)}_{j+\frac{1}{2}} := \alpha_0 u^{(0)}_{j+\frac{1}{2}} + \alpha_{0,1} u^{(1)}_{j+\frac{1}{2}}, \tag{26a}$$

$$u^{(1,2)}_{j+\frac{1}{2}} := \alpha_{1,2} u^{(1)}_{j+\frac{1}{2}} + \alpha_2 u^{(2)}_{j+\frac{1}{2}}. \tag{26b}$$

We consider two possible choices for the linear weights of the inner scheme, see Table 2. The first is the fourth-order linear combination which is possible on the four-point stencil. The second choice consists of placing the superfluous weight onto the middle substencil, i.e., using the approximation $u^{(k)}_{j+\frac{1}{2}} \approx u^{(1)}_{j+\frac{1}{2}}$ for $k = 0, 2$. The fourth-order choice is motivated from an order-of-convergence perspective, while the third-order choice comes from a spectral point of view, see Section 3.

The nonlinear weights must at all times sum to unity to ensure consistency. Thus, any correction we introduce must be incorporated into the unnormalised linear weights and still work after normalisation. Furthermore,

	4th	3rd
α_0	$\frac{1}{4}$	$\frac{1}{10}$
$\alpha_{0,1}$	$\frac{3}{4}$	$\frac{9}{10}$
$\alpha_{1,2}$	$\frac{1}{2}$	$\frac{7}{10}$
α_2	$\frac{1}{2}$	$\frac{3}{10}$

Table 2: Possible choices for the inner scheme.

what is happening in stencil S_2 must influence both stencils S_0 and S_1 and mutatis mutandis for stencil S_0. It follows that the corrections must be functions of multiple smoothness indicators. As a final note, we have seen that in (25) that in the appropriate limit, the nonlinear weights are simply a redistribution of the linear weights. All these considerations suggest that the corrections should grow large at the same rate, but with some relative proportions c_0 and c_2. The relative proportions can be found as

$$\alpha_0 : \alpha_{0,1} = c_0\gamma_0 : \gamma_1, \tag{27a}$$

$$\alpha_{1,2} : \alpha_2 = \gamma_1 : c_2\gamma_2. \tag{27b}$$

$$\tag{27c}$$

We can thus compute the relative proportions using the inner weights suggested in Table 2, see Table 3. The correction on the discontinuous stencil should not grow and will consequently become very small after normalisation.

	4th	3rd
c_0	2	$\frac{2}{3}$
c_2	2	$\frac{6}{7}$

Table 3: Relative proportions for the 4th order inner scheme and the 3rd order inner scheme which places the superfluous weight on the middle stencil.

We shall now briefly summarize the design constraints for the correction.

1. The correction must be multiplied with the unnormalised weights.
2. Wherever the solution is smooth on the full stencil, the correction should be close to unity.

3. The corrections must grow large whenever only two adjacent substencils are smooth. The rate at which the corrections grow large must adjust the proportions of the linear weights.
4. The corrections on S_k cannot be a function of only β_k.

We shall now give two examples of how to apply the design method as presented. We explicitly construct an embedded scheme which uses WENO-JS as the outer scheme and an embedded scheme with WENO-Z as the outer scheme.

2.1. Embedded WENO-JS

We will now show how to construct embedded WENO schemes using the WENO-JS scheme as an outer scheme. We will assume the inner weights α_0, $\alpha_{0,1}$, $\alpha_{1,2}$ and α_2 are given, e.g., chosen from Table 2. From the inner weights, we can find their relative proportions as measured against the outer weights by (27), see Table 3. The correction factors can be constructed by considering ratios of the smoothness indicators. In fact, from (11), we find for $k \neq l$

$$\frac{\beta_k}{\beta_l} = \begin{cases} 1 + \mathcal{O}(\Delta x^2) & \text{if } \beta_k = \mathcal{O}(\Delta x^2) \text{ and } \beta_l = \mathcal{O}(\Delta x^2), \\ \mathcal{O}(\frac{1}{\Delta x^2}) & \text{if } \beta_k = \mathcal{O}(1) \text{ and } \beta_l = \mathcal{O}(\Delta x^2), \\ \mathcal{O}(\Delta x^2) & \text{if } \beta_l = \mathcal{O}(1) \text{ and } \beta_k = \mathcal{O}(\Delta x^2). \end{cases} \tag{28}$$

To avoid division by zero, we introduce a small parameter δ. Borges et al. [2] argued that whenever δ is chosen exceedingly small, say 10^{-40}, we may analyse our scheme as if $\delta = 0$. Thus, we may implement ratios such as (28) by using $\frac{\beta_k}{\beta_l + \delta}$. The WENO-JS unnormalised weights will be indicated with the superscript JS. We cannot simply multiply the WENO-JS weights with a ratio such as 28 since then they cannot satisfy demands 2 and 3 at the same time. Adding a constant factor, however, does work. Constructing the corrections as indicated gives

$$\tilde{\omega}_0 = \tilde{\omega}_0^{\mathrm{JS}} \left(a_0 + c_0 \frac{\beta_2}{\beta_0 + \delta} \right), \tag{29a}$$

$$\tilde{\omega}_1 = \tilde{\omega}_1^{\mathrm{JS}} \left(1 + \frac{\beta_2}{\beta_1 + \delta} + \frac{\beta_0}{\beta_1 + \delta} \right), \tag{29b}$$

$$\tilde{\omega}_2 = \tilde{\omega}_2^{\mathrm{JS}} \left(a_2 + c_2 \frac{\beta_0}{\beta_2 + \delta} \right), \tag{29c}$$

where the numbers a_0 and a_2 are still to be determined. The reason we do not take another parameter a_1 is to minimize the number of parameters. The numbers a_0 and a_2 must be such that whenever the solution is smooth on the whole stencil S, we obtain $\tilde{\omega}_k = \tilde{\omega}_k^{JS}(A + \mathcal{O}(\Delta x^2))$, where A is a constant that does not depend on k. This enforces that the scheme is equal, up to a term of order $\mathcal{O}(\Delta x^4)$ to the outer scheme whenever the solution is smooth. Using (28) and assuming the solution is smooth on the entire stencil S, we find

$$\tilde{\omega}_0 = \tilde{\omega}_0^{\mathrm{JS}} \left(a_0 + c_0 + \mathcal{O}(\Delta x^2)\right), \tag{30a}$$

$$\tilde{\omega}_1 = \tilde{\omega}_1^{\mathrm{JS}} \left(3 + \mathcal{O}(\Delta x^2)\right), \tag{30b}$$

$$\tilde{\omega}_2 = \tilde{\omega}_2^{\mathrm{JS}} \left(a_2 + c_2 + \mathcal{O}(\Delta x^2)\right). \tag{30c}$$

Thus, we should have $a_0 = 3 - c_0$ and $a_2 = 3 - c_2$. As it is, these coefficients are enough to make the scheme work, as any common constant is divided out by the normalisation step. However, for aesthetic reasons, we choose to divide all the weights by 3, such that the correction is ordinarily close to unity. This leads us to unnormalised weights given by

$$\tilde{\omega}_0 = \tilde{\omega}_0^{\mathrm{JS}} \tfrac{1}{3} \left(3 - c_0 + c_0 \frac{\beta_2}{\beta_0 + \delta}\right), \tag{31a}$$

$$\tilde{\omega}_1 = \tilde{\omega}_1^{\mathrm{JS}} \tfrac{1}{3} \left(1 + \frac{\beta_2}{\beta_1 + \delta} + \frac{\beta_0}{\beta_1 + \delta}\right), \tag{31b}$$

$$\tilde{\omega}_2 = \tilde{\omega}_2^{\mathrm{JS}} \tfrac{1}{3} \left(3 - c_2 + c_2 \frac{\beta_0}{\beta_2 + \delta}\right). \tag{31c}$$

A WENO scheme should always give a convex combination, meaning positive weights, in order to be essentially non-oscillatory. Hence, the embedded WENO scheme (31) is essentially nonoscillatory if

$$0 \leq c_i < 3, \quad i = 0, 2, \tag{32}$$

where the choice $c_i = 0$ corresponds to using simply the WENO-JS scheme. Note that the relative proportions displayed in Table 3 satisfy these condition. Any selection of c_0 and c_2 from Table 3 will therefore result in an essentially nonoscillatory scheme.

Let us denote the corrections to the WENO-JS unnormalised weights as g_i, $i = 0, 1, 2$, such that the unnormalised weights read $\tilde{\omega}_i = \tilde{\omega}_i^{\mathrm{JS}} g_i$. Then we

have that $g_i = 1 + \mathcal{O}(\Delta x^2)$ whenever the solution is smooth on the whole stencil S, and thus

$$\tilde{\omega}_k = \tilde{\omega}_k^{\text{JS}} \left(1 + \mathcal{O}(\Delta x^2)\right). \tag{33}$$

However, for smooth solutions we also know that $\tilde{\omega}_k^{\text{JS}} = \gamma_k + \mathcal{O}(\Delta x^2)$. We conclude that for smooth solutions, the embedded WENO scheme with outer WENO-JS is simply equal to the WENO-JS, up to the fourth-order term. Unlike the regular WENO-JS scheme, we may choose $p = 0$, i.e., $\tilde{\omega}_k^{\text{JS}} = \gamma_k$, and still obtain a stable scheme. In fact, any $p > 0$ tends to homogenise the effects, as Henrick et al. [9] pointed out.

Now we shall examine the case when the stencil S contains a discontinuity such that β_0 or β_2 become $\mathcal{O}(1)$. Let us assume that that $\beta_0 = \beta_1$ and that the discontinuity is in substencil S_2, the other case being completely similar. This allows us to introduce

$$z = \frac{\beta_2}{\beta_0} = \frac{\beta_2}{\beta_1}, \tag{34}$$

where we shall ignore the small number δ. Note that we can also choose $\beta_0 \neq \beta_1$ and introduce two variables, but this makes the analysis needlessly complicated. As we shall see, all the interesting cases are captured in z. Choosing $p = 0$, we can then write the unnormalised nonlinear weights as follows,

$$\tilde{\omega}_0 = \gamma_0 \tfrac{1}{3}(3 - c_0 + c_0 z), \tag{35a}$$
$$\tilde{\omega}_1 = \gamma_1 \tfrac{1}{3}(2 + z), \tag{35b}$$
$$\tilde{\omega}_2 = \gamma_2 \tfrac{1}{3}(3 - c_2 + \tfrac{c_2}{z}). \tag{35c}$$

We can thus write the nonlinear weight ω_0, for instance, as

$$\omega_0 = \frac{\gamma_0(3 - c_0 + c_0 z)}{\gamma_0(3 - c_0 + c_0 z) + \gamma_1(2 + z) + \gamma_2(3 - c_2 + \frac{c_2}{z})}, \tag{36}$$

where the common factor $\frac{1}{3}$ cancels out. The other nonlinear weights can also be written as rational functions of z, each exhibiting similar properties. Since z is essentially one instance of a ratio as presented in (28), we shall investigate each of the three cases.

Using $z = 1 + \mathcal{O}(\Delta x^2)$ in (36) gives

$$\omega_0 = \frac{\gamma_0 + \mathcal{O}(\Delta x^2)}{\gamma_0 + \gamma_1 + \gamma_2 + \mathcal{O}(\Delta x^2)} = \gamma_0 + \mathcal{O}(\Delta x^2). \tag{37}$$

By repeating the argument for ω_1 and ω_2, we find that $\omega_i = \gamma_i + \mathcal{O}(\Delta x^2)$ whenever $\beta_i = \mathcal{O}(\Delta x^2)$. The second case, $z = \mathcal{O}(\Delta x^2)$ leaves us with

$$\omega_0 = \frac{\gamma_0 \left(3 - c_0\right) + \mathcal{O}(\Delta x^2)}{\gamma_0(3 - c_0) + 2\gamma_1 + \gamma_2(3 - c_2) + \mathcal{O}(\frac{1}{\Delta x^2})} = \frac{\mathcal{O}(\Delta x^2)}{\mathcal{O}(1)} = \mathcal{O}(\Delta x^2). \quad (38)$$

A similar calculation for ω_1 and ω_2 shows that $\omega_1 = \mathcal{O}(\Delta x^2)$ and $\omega_2 = 1 + \mathcal{O}(\Delta x^2)$. Finally, the third case, $z = \mathcal{O}(\frac{1}{\Delta x^2})$, yields

$$\omega_0 = \frac{\gamma_0 c_0 \frac{C}{\Delta x^2} + \mathcal{O}(1)}{(\gamma_0 c_0 + \gamma_1)\frac{C}{\Delta x^2} + \mathcal{O}(1)} = \frac{c_0\gamma_0 + \mathcal{O}(\Delta x^2)}{c_0\gamma_0 + \gamma_1 + \mathcal{O}(\Delta x^2)} = \alpha_0 + \mathcal{O}(\Delta x^2), \quad (39)$$

where the last equality comes from the definition of c_0. One can also show that $\omega_1 = \alpha_{0,1} + \mathcal{O}(\Delta x^2)$ and $\omega_2 = \mathcal{O}(\Delta x^2)$.

We conclude that the embedded WENO-JS scheme given by (31) is equivalent to the standard WENO-JS scheme for smooth solutions or discontinuities contained in S_1. When there are two adjacent smooth substencils and third one is not smooth, we obtain the inner scheme. In the form of (36), it becomes clear that conventional WENO schemes only treat the two cases where $z \approx 1$ and $z \approx 0$. Adding an extra parameter provides us with the possibility to choose the value of the weights in the limit of large z.

One further interesting note is that near critical points where $\partial_x u = 0$, where $\beta = D\Delta x^4 + \mathcal{O}(\Delta x^5)$. The embedded WENO-JS scheme with $p = 0$ should in that case provide $\omega_k = \gamma_k + \mathcal{O}(\Delta x)$. Hence, the embedded scheme should also avoid any loss of rate of convergence near such points. We have, however, not investigated this property.

The effects of the embedding technique can be visualized by considering the function $u(x) = \sin(5\pi x)$ on the interval $[-1, 1]$ and applying the various WENO methods. We have used the fourth-order inner scheme, i.e., $c_0 = c_2 = 2$. Furthermore, we have set $\tilde{\omega}_k^{\text{JS}} = \gamma_k$, $\delta = 10^{-40}$. We shall refer to this scheme as the WENO-45 scheme, as it switches between fourth and fifth-order modes. Finally, we have chosen 200 grid points. Using these parameters, we plot the linear and nonlinear weights of both schemes, see Figure 3.

One feature which is immediately clear from the figures, is that the weights of the WENO-45 scheme oscillate with a smaller amplitude around the linear weights. However, this is merely a side-effect, although a pleasant one.

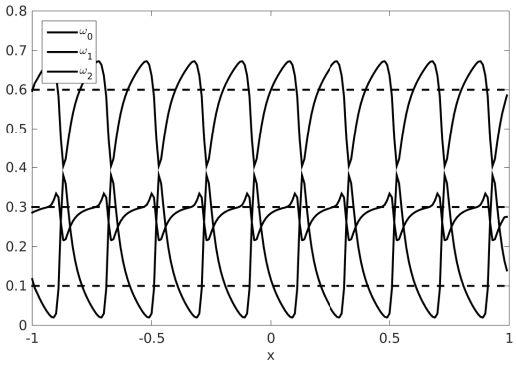

Figure 3a: WENO-JS.

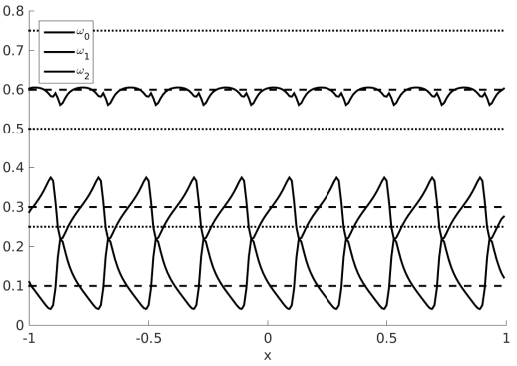

Figure 3b: WENO-45.

Figure 3: Linear (dashed) and nonlinear (solid) weights for the WENO-JS and the WENO-45 scheme with 200 grid points. The dashed lines indicate the outer scheme linear weights, the dotted lines indicate the inner scheme linear weights.

2.2. Embedded WENO-Z

A more contemporary version of a WENO scheme is represented by the WENO-Z scheme of Borges et al. [2]. As mentioned earlier, the WENO-JS scheme has the property that $\omega_k = \gamma_k + \mathcal{O}(\Delta x^2)$ for smooth solutions. Although popular, one can show that near points where $\partial_x u = 0$, the WENO-JS scheme only provides third-order accuracy, as pointed out by Henrick et al. [9]. The WENO-Z scheme corrects for this flaw by having $\omega_k^{\mathrm{Z}} = \gamma_k + \mathcal{O}(\Delta x^3)$ for smooth solutions. Consequently, at points where $\partial_x u = \mathcal{O}(\Delta x)$, the WENO-Z scheme has $\omega_k^{\mathrm{Z}} = \gamma_k + \mathcal{O}(\Delta x)$, which results in fourth-order accuracy. A side-effect of the new weights is faster convergence to the linear weights in smooth regions. This also results in sharper resolution of discontinuities.

The WENO-Z scheme accomplishes these features by introducing a new smoothness indicator, $\tau := |\beta_0 - \beta_2|$. According to (11), $\tau = \mathcal{O}(\Delta x^5)$, while the new unnormalissed weights are defined as

$$\tilde{\omega}_k^{\mathrm{Z}} = \gamma_k \left(1 + \frac{\tau}{\beta_k + \varepsilon_{\mathrm{Z}}}\right), \tag{40}$$

where ε_{Z} is a small parameter, usually taken to be 10^{-40}. Embedding an inner scheme into the WENO-Z scheme is particularly easy, since τ furthermore exhibits the property that $\tau = \mathcal{O}(1)$ when either β_0 or β_2 become $\mathcal{O}(1)$.

Furthermore, the unnormalised weights satisfy all the design constraints already, except that they do not correct the proportions in case β_0 or β_2 become $\mathcal{O}(1)$. We may indeed multiply the unnormalised weights with a correction factor as we have done with the WENO-JS scheme. However, since the unnormalised weights exhibit the desirable properties already, we may simply introduce the relative proportions as follows,

$$\tilde{\omega}_0 = \gamma_0 \left(1 + c_0 \frac{\tau}{\beta_0 + \varepsilon_{\mathrm{Z}}}\right), \tag{41a}$$

$$\tilde{\omega}_1 = \gamma_1 \left(1 + \frac{\tau}{\beta_1 + \varepsilon_{\mathrm{Z}}}\right), \tag{41b}$$

$$\tilde{\omega}_2 = \gamma_2 \left(1 + c_2 \frac{\tau}{\beta_2 + \varepsilon_{\mathrm{Z}}}\right). \tag{41c}$$

The relative proportions are again given in Table 3. Whenever the solution is smooth, we obtain $\omega_k = \gamma_k + \mathcal{O}(\Delta x^3)$, since ε_{Z} is exceedingly small. Furthermore, if either $\beta_2 = \mathcal{O}(1)$ or $\beta_0 = \mathcal{O}(1)$, we obtain the inner scheme.

Stability of the scheme is not as much of an issue as with the embedded WENO-JS, since we now have positive weights whenever

$$c_i > 0, \quad i = 0, 2. \tag{42}$$

As a final note on the embedded WENO-Z schemes, we note that we can insert an arbitrary constant B such that

$$\tilde{\omega}_0 = \gamma_0 \left(1 + B c_0 \frac{\tau}{\beta_0 + \varepsilon_{\mathrm{Z}}}\right), \tag{43a}$$

$$\tilde{\omega}_1 = \gamma_1 \left(1 + B \frac{\tau}{\beta_1 + \varepsilon_{\mathrm{Z}}}\right), \tag{43b}$$

$$\tilde{\omega}_2 = \gamma_2 \left(1 + B c_2 \frac{\tau}{\beta_2 + \varepsilon_{\mathrm{Z}}}\right). \tag{43c}$$

The constant B does not play a role whenever $\beta_k = \mathcal{O}(1)$ for $k = 0, 2$, since it then cancels out in the normalisation step. However, it does play a role in the "error constant" with respect to the linear weights. Therefore, it might be advantageous to have the embedded scheme be as close as possible to the standard scheme in the sense that we minimise

$$(Bc_0 - 1)^2 + (B - 1)^2 + (Bc_2 - 1)^2. \tag{44}$$

One can show that

$$B = \frac{1 + c_0 + c_2}{1 + c_0^2 + c_2^2} \tag{45}$$

minimises the expression (44).

We apply the WENO-Z and WENO-Z45 (WENO-Z outer with fourth-order inner scheme) schemes to the test function $u(x) = \sin(5\pi x)$ to examine the behaviour of the weights. The WENO-Z45 has the unnormalised weights defined by (41) with $c_0 = c_2 = 2$, thus resulting in fourth-order accuracy whenever possible. The results are plotted in 4.

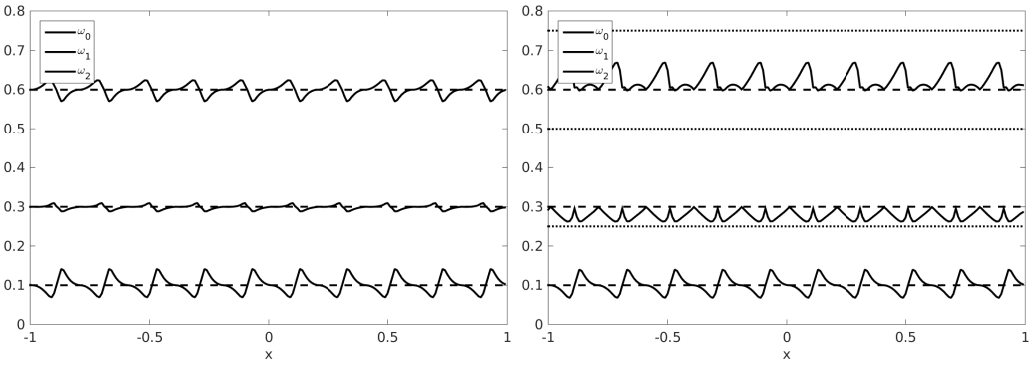

Figure 4a: WENO-Z.

Figure 4b: WENO-Z45.

Figure 4: Linear (dashed) and nonlinear (solid) weights for the WENO-Z and the WENO-Z45 scheme with 200 grid points. Recall that $\gamma_0 = 0.1$, $\gamma_1 = 0.6$ and $\gamma_2 = 0.3$.

The first feature that becomes clear from the figure is that the oscillations in the weights are larger for the embedded method. This is an unfortunate by-product of the embedding process. However, the second, and perhaps more interesting feature, is that the WENO-Z45 weights are bounded, for this particular example, by the fourth-order linear weights. Another feature we can clearly distinguish is that the WENO-Z weights are symmetrical, while the WENO-Z45 weights oscillate asymmetrically, indicating a preferred direction. This preferred direction is, of course, towards the inner weights.

2.3. Notation of embedded schemes

As indicated earlier, the relative proportions c_0 and c_2 can be chosen independently. Thus, we may choose a fourth-order inner scheme on $S_{1,2}$, while on $S_{0,2}$ we may place the superfluous weight on the middle stencil. The

two variants discussed together with the choices offered results in 8 possible schemes. To clarify which scheme is being used at the particular time, we propose the following notation. We shall write the outer scheme with the relative proportions in parenthesis: WENO-JS(c_0, c_2) and WENO-Z(c_0, c_2). In special cases, we shall explicitly name a scheme, such as the schemes which have fourth-order inner schemes WENO-45 := WENO-JS(2,2) and WENO-Z45 := WENO-Z(2,2).

3. Spectral properties

The embedded WENO schemes may be investigated by analysing their spectral properties. The inner scheme activates whenever β_0 or β_2 become significantly larger than the other two smoothness indicators. In terms of sinusoidal functions, one would expect this to happen in the medium-range of wave numbers. Thus, the spectral properties of a WENO scheme in this regime can be improved by embedding an inner scheme. At very high wave numbers, all WENO schemes revert to what is essentially an ENO scheme.

As an example, we will show that we can reduce the dissipation of a WENO scheme by embedding an inner scheme. This is particularly useful when working with smooth solutions. On the other hand, when working with sharply varying or even discontinuous solutions, one may wish to increase dissipation to obtain greater stability.

One can investigate the spectral properties of WENO scheme by analysing the underlying linear schemes [18]. We can interpret the WENO schemes as a linear combination of the underlying third-order upwind schemes, where the weights vary with the wave numbers. This way, we may find upper and lower bounds for the spectral curves. We consider here plane wave initial conditions to the linear advection equation,

$$\frac{\partial u}{\partial t} + \frac{\partial u}{\partial x} = 0. \tag{46}$$

Linear schemes can be represented by a set of coefficients l_n such that

$$\frac{\partial u}{\partial x}(x_j, t) \approx \frac{1}{\Delta x} \sum_k l_n u(x_{j+k}, t) =: L\big(u(x_j, t)\big). \tag{47}$$

For the standard five-point WENO schemes, there are four such linear schemes, three for the three-point substencils and one for the full five-point stencil.

For embedded schemes, there are six underlying linear schemes, the added two are both defined on a four-point stencil. By inserting a plane wave $u(x,t) = \exp(\mathrm{i}(\kappa x - \omega t))$, we can define the modified wave number κ^*:

$$\Delta x L\big(u(x_j,t)\big) = \sum_k l_n e^{\mathrm{i}\kappa\Delta x k} u(x_j,t) =: \mathrm{i}\kappa^* u(x_j,t)\Delta x. \tag{48}$$

The modified wave number κ^* is a complex number, its real part being related to the dispersion, while the imaginary part is related to dissipation. After application of the method of lines, the numerical solution u^* satisfies

$$\frac{\mathrm{d}}{\mathrm{d}t} u^*(x_j,t) = -\mathrm{i}\kappa^* u(x_j,t). \tag{49}$$

This ODE can be integrated using strong stability preserving Runge-Kutta methods like SSPRK(3,3) or SSPRK(5,4). In general, we can write an RK method as

$$u_j^{n+1} = u_j^n + \Delta t \mathbf{b}^T \mathbf{K}, \tag{50}$$

where the vector $\mathbf{K}$ consists of the intermediate stages, which satisfy

$$\mathbf{K} = -L\big(u_j^n \mathbf{1} + \Delta t A\mathbf{K}\big) = -\mathrm{i}\kappa^*(u_j^n \mathbf{1} + \Delta t A\mathbf{K}), \tag{51}$$

where $\mathbf{1} := (1,1,\ldots,1)^T$ and A is the Butcher array. Thus, for any general RK method applied to (49), we find

$$\mathbf{K} = -\mathrm{i}\kappa^* u_j^n \left(I + \mathrm{i}\kappa^* \Delta t A\right)^{-1} \mathbf{1}. \tag{52}$$

It is common to scale the wave numbers with the grid size to turn it into a phase angle $\varphi := \kappa\Delta x$ and $\varphi^* := \kappa^*\Delta x$. Thus, we find for a single time step evolution due to the RK method,

$$u_j^{n+1} = u_j^n \left(1 - \mathrm{i}\varphi^* c \mathbf{b}^T \left(I + \mathrm{i}\varphi^* c A\right)^{-1} \mathbf{1}\right), \tag{53}$$

where c is the CFL number $c := \frac{\Delta t}{\Delta x}$. For explicit RK methods, the matrix A is strictly lower triangular and therefore the matrix $I + \mathrm{i}\kappa^*\Delta t A$ is in row-echelon form. From (53), we see that a single time step is simply a multiplication with a constant, possibly a complex number, given by

$$\lambda(\varphi) = 1 - \mathrm{i}\varphi^* c \mathbf{b}^T \left(I + \mathrm{i}\varphi^* c A\right)^{-1} \mathbf{1}. \tag{54}$$

Thus, a single time step for the numerical solution is given by $u_j^{n+1} = \lambda u_j^n$. However, a single time step of the plane wave is given by

$$u(x_j, t^{n+1}) = e^{-\mathrm{i}\omega\Delta t} u(x_j, t^n). \tag{55}$$

If we now set $u_j^n = u(x_j, t^n)$, we can compare the numerical solution at $t = t^{n+1}$ to the exact plane wave and find that

$$u_j^{n+1} = \lambda e^{\mathrm{i}\omega\Delta t} u(x_j, t^{n+1}) = |\lambda| e^{\mathrm{i}(c\varphi+\theta)} u(x_j, t^{n+1}), \tag{56}$$

where θ is the argument of λ in the complex plane. The absolute value of λ determines the dissipation, $|\lambda| = 1$ being a nondissipative scheme. The argument of λ determines the phase error in the numerical approximation, thus relating to dispersion. Therefore, an exact scheme has $|\lambda| = 1$ and $\theta + c\varphi = 0$.

Let us first investigate the basic spectral properties of the three possible third-order approximations and the fifth-order linear combination, see Figure 5. A WENO scheme will give a fifth-order approximation for smooth solutions, while a third-order approximation for rapidly varying solutions. Thus, we expect the WENO scheme to follow the fifth-order curves for low wave numbers and the third-order curves for high wave numbers. These considerations give us a qualitative understanding of WENO methods. The embedded methods will switch to their inner scheme for mid-range wave numbers.

Let us now study the inner schemes, which are four-point linear schemes given by (26), completed by Table 2. The resulting dispersion and dissipation curves are presented in Figure 6. An important thing to note is that all inner schemes do not support parasitic wave modes, since $|\lambda| \leq 1$ across the whole range. Thus, the inner schemes will improve the stability of a WENO scheme.

What becomes clear from the curves is that one can certainly influence the spectral properties of the scheme. However, the dispersion curve for any inner scheme on $S_{1,2} = S_1 \cup S_2$ is roughly the same. This is due to the fact that the real part of the modified wave numbers on these stencils is equal. Furthermore, the fourth-order choice on $S_{1,2}$ results in very little dissipation. In fact, the little dissipation present comes solely from the time integrator, since S_1 and S_2 are symmetrical around the point $x_{j+\frac{1}{2}}$. Alternatively, the dissipation can also be increased as compared to standard issue WENO schemes, which can provide advantages in terms of stability. Also, it should be noted that the curve corresponding to $c_0 = \frac{2}{3}$ gives a dispersion curve which is very close to the fifth-order dispersion curve. Therefore,

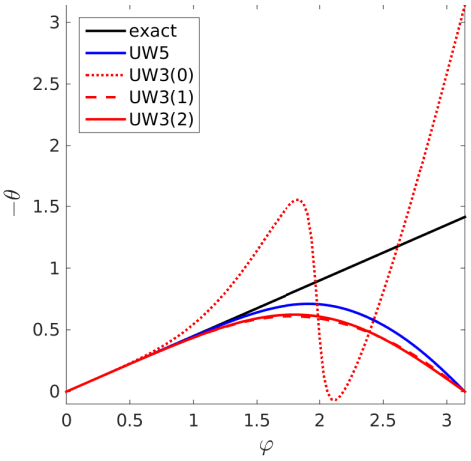

Figure 5a: Dispersion.

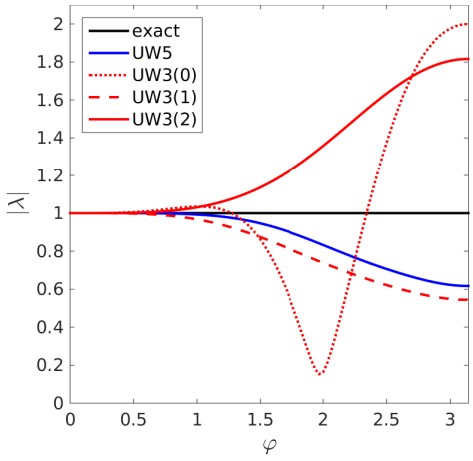

Figure 5b: Dissipation.

Figure 5: Dispersion (a) and dissipation (b) curves for the underlying linear schemes. UW5 indicates the fifth-order upwind approximation. The label in parenthesis for the UW3 schemes indicate on what stencil it works, thus UW3(i) works on S_i.

this justifies this particular choice, as it reduces the phase difference near discontinuities.

We shall now demonstrate the influence of the innner scheme on the spectral properties by some numerical examples. We solve the linear advection equation (46) using several variants of WENO schemes on a periodic domain with the initial condition a sine wave. We pick as the wave number $\kappa = 10\pi$, thus the initial condition is given by

$$u_0(x) = \sin(10\pi x). \tag{57}$$

As the initial condition is smooth, we shall use the inner scheme to reduce dissipation. Hence, we shall compare the standard WENO-JS and WENO-Z schemes to the WENO-JS($\frac{2}{3}$,2) and WENO-Z($\frac{2}{3}$,2) variants. We integrate the advection equation for 64 time units using the SSPRK(3,3) method and examine the amplitude of the numerical solutions, see Figure 7.

All the WENO schemes are, in this case, still solving with fifth-order accuracy in most of the domain. The WENO-Z($\frac{2}{3}$,2) scheme proves to be the least dissipative, followed by the WENO-Z scheme. Moreover, for this wave number the WENO-JS scheme overestimates the solution, as it is reverting to the third-order upwind scheme. The WENO-JS($\frac{2}{3}$,2) has the most

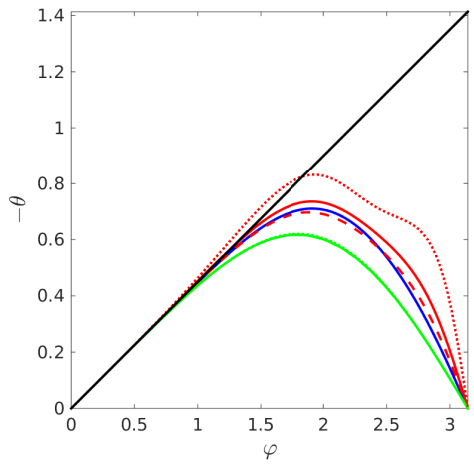

Figure 6a: Dispersion.

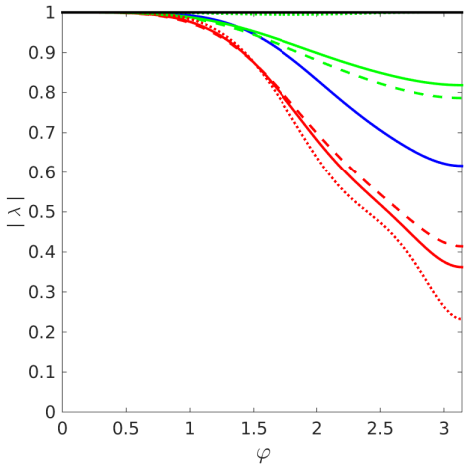

Figure 6b: Dissipation.

Figure 6: Dispersion (a) and dissipation (b) curves for the inner scheme. The blue curves are the fifth-order curves, the red curves are schemes working on $S_0 \cup S_1$ and the green curves work on $S_1 \cup S_2$. The solid curves represent $c_0 = c_2 = 1$, the dashed curves represent $(c_0, c_2) = (\frac{2}{3}, \frac{6}{7})$ and the dotted curves represent $c_0 = c_2 = 2$.

amount of dissipation, which proves our assertion that the embedded WENO schemes suppress parasitic wave modes. Dispersive effects remain minimal in all schemes. Here, it also becomes more interesting to plot the error, see Figure 8. We clearly see that the WENO-Z($\frac{2}{3}$,2) scheme exhibits the smallest error at every point in the domain. At most points, the WENO-Z($\frac{2}{3}$,2) scheme has an error which is roughly an order of magnitude lower than its standard counterparts.

We will now investigate a higher wave number. We use the initial condition

$$u_0(x) = \sin(20\pi x). \tag{58}$$

The results are plotted in Figure 9. In this case, dispersive effects start to be visible. Furthermore, due to the rapid variations, the WENO schemes are resorting to their underlying lower order schemes. It becomes clear that the WENO-Z scheme has a lot of dissipation at higher wave numbers. In this particular example, the WENO-Z scheme exhibits so much dampening that the oscillations are scarcely visible. The WENO-JS($\frac{2}{3}$,2) scheme also exhibits a large amount of dissipation for this wave number. The WENO-

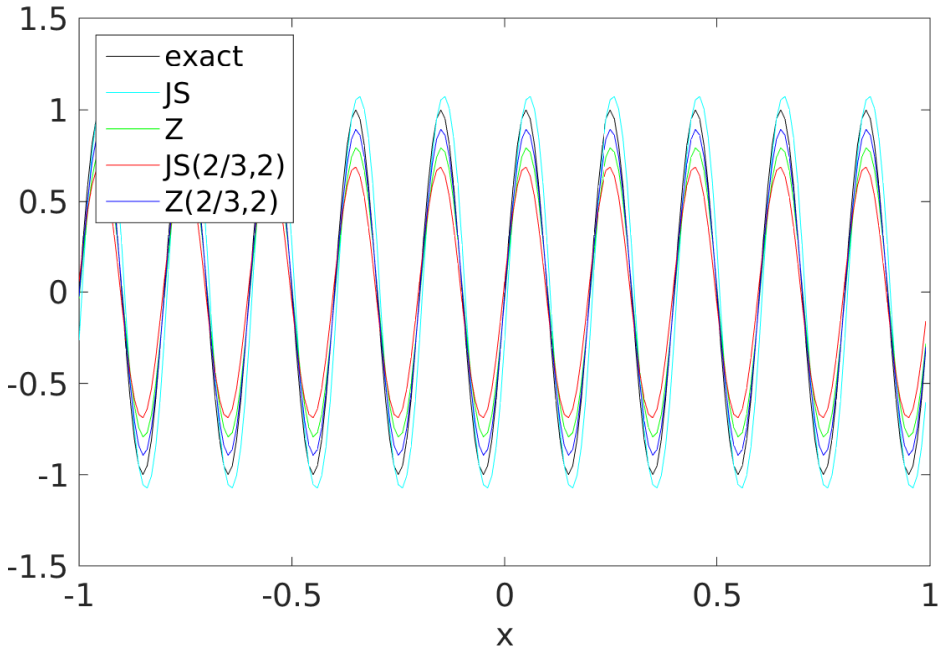

Figure 7: Sine wave with wave number $\kappa = 10\pi$ at $t = 64$ on a periodic domain with 200 grid points and a CFL number of 0.45.

Z($\frac{2}{3}$,2) scheme still shows some of the oscillations, which means that the inner scheme causes a decrease in dissipation.

4. Numerical experiments

As a final demonstration of the embedded WENO methods, we will here perform some numerical experiments. An examples of a hyperbolic equation and an example of a hyperbolic system are presented. First, we shall take the linear advection equation with constant velocity field. Second, several cases of the shallow water equations are solved. In all examples we compare our methods to the WENO-JS and the WENO-Z scheme.

4.1. Linear advection equation

We consider here the linear advection equation, i.e.,

$$\frac{\partial u}{\partial t} + \frac{\partial u}{\partial x} = 0, \tag{59}$$

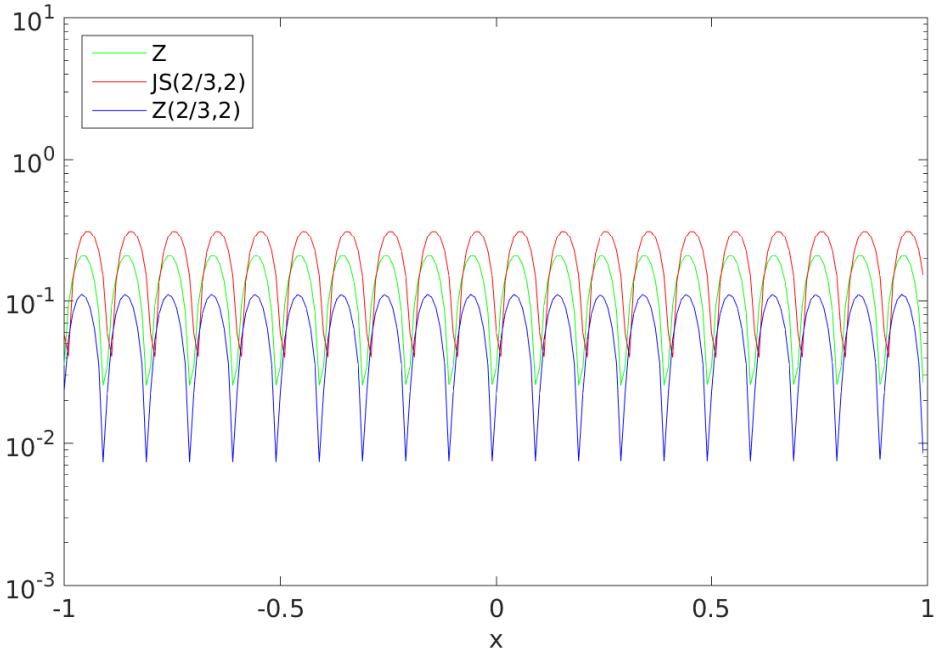

Figure 8: Error of the sine wave with wave number $\kappa = 10\pi$ at $t = 64$ on a periodic domain with 200 grid points and a CFL number of 0.45.

on $(x, t) \in [-1, 1] \times [0, 8]$. We use periodic boundary conditions, such that the initial condition is transported around four times and ends up where it started. Thus, the final state is equal to the initial condition, i.e., $u(x, 8) = u_0(x)$. As an initial condition, we take the fairly standard test which uses a Gaussian, a square, a triangle and half an ellipse. This setup is sometimes referred to as the Shu linear test, introduced in [1]. The initial condition is given by

$$u_0(x) = \begin{cases} \frac{1}{6}\left(G(x;\beta,z-\epsilon) + G(x;\beta,z+\epsilon) + G(x;\beta,z)\right) & -0.8 \leq x \leq -0.6, \\ 1 & -0.4 \leq x \leq -0.2, \\ 1 - |10(x-0.1)| & 0 \leq x \leq 0.2, \\ \frac{1}{6}\left(F(x;\alpha,a-\epsilon) + F(x;\alpha,a+\epsilon) + 4F(x;\alpha,a)\right) & 0.4 \leq x \leq 0.6, \\ 0 & \text{otherwise}, \end{cases} \tag{60a}$$

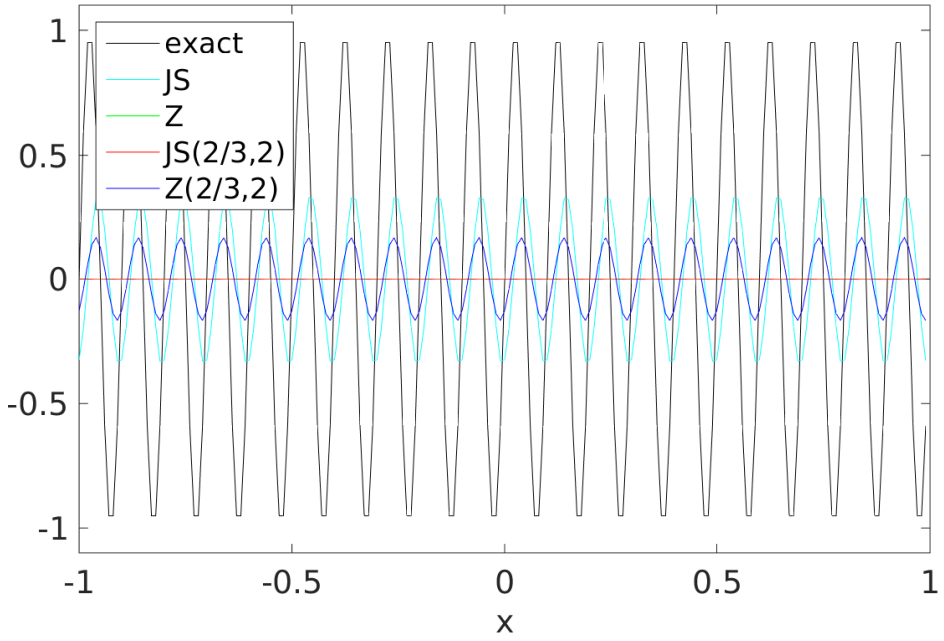

Figure 9: Sine wave with wave number $\kappa = 20\pi$ at $t = 64$ on a periodic domain with 200 grid points and a CFL number of 0.45.

where G and F are given by

$$G(x;\beta,z) := \exp\big(-\beta(x-z)^2\big), \tag{60b}$$

$$F(x;\alpha,z) := \sqrt{\max\big(1-\alpha^2(x-a)^2,0\big)}. \tag{60c}$$

The parameters are as follows: $z = -0.7$, $a = 0.5$, $\alpha = 10$, $\epsilon = \frac{1}{200}$, and $\beta = \frac{\ln 2}{36\epsilon^2}$. One of the pervasive features of this test is the compact support of the initial condition. In fact, the shapes have non-overlapping supports. Thus, we need the numerical solutions to converge to zero as quickly as possible in between each shape. Thus, the third-order choice where the superfluous weight is shifted to the middle stencil offers the best choice heuristically. However, this will also provide more dissipation compared to the other options.

Let us start with the embedded schemes that use WENO-JS as its outer scheme, we expect to see better performance near discontinuities. Moreover, we also expect discontinuities in the first derivative to be captured better. The Shu linear test has both types of discontinuities, as well as smooth

transitions. The embedded schemes switch to their inner schemes close to the edge of the support of each shape, and hence are able to capture it better, see Figure 10.

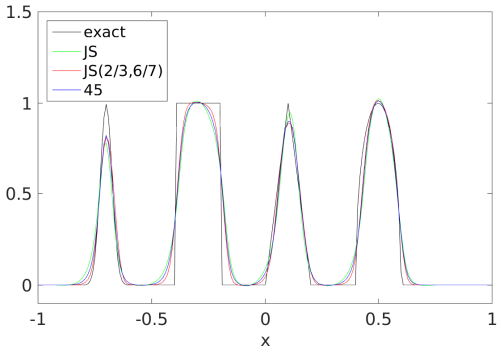

Figure 10a: Numerical solutions to the advection equation.

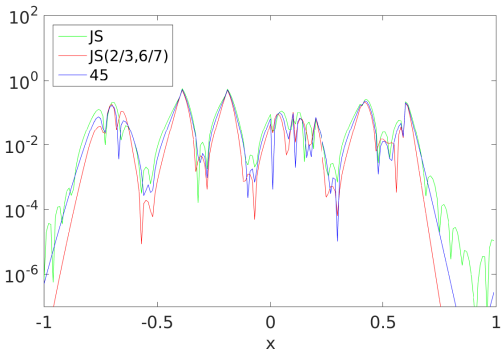

Figure 10b: Error compared to the exact solution.

Figure 10: Results for the linear advection equation using WENO-JS (green) and its embedded variants, WENO-45 (blue) and WENO-JS($\frac{2}{3},\frac{6}{7}$) (red). Solutions were computed on a periodic domain at $t = 8$, using 200 grid points and a CFL number of 0.45.

It becomes clear, also from Figure 10b, that the embedded WENO schemes perform better in almost every part of the domain. However, it should be noted that the WENO-45 scheme seems to perform best within each smoothly varying region, whereas the WENO-JS($\frac{2}{3},\frac{6}{7}$) scheme captures the compact support of each shape the best. The WENO-JS($\frac{2}{3},\frac{6}{7}$) scheme seems to decay to zero the fastest in between each shape. However, the WENO-45 scheme has less dissipation and captures the maxima better in general. Interestingly, the WENO-JS scheme give the best representation of the peak of the triangle. However, in all other parts of the triangle, the embedded schemes provide a smaller error.

Next, we shall examine the numerical performance of embedded schemes with the WENO-Z scheme as the outer scheme. By the same argument as presented previously, we expect the embedded schemes to perform better near discontinuities in the solution and its derivative. The results are plotted in Figure 11.

The figures show how the WENO-Z($\frac{2}{3},\frac{6}{7}$) captures the compact support of the shapes the best. Again, this variant decays the fastest to zero in the

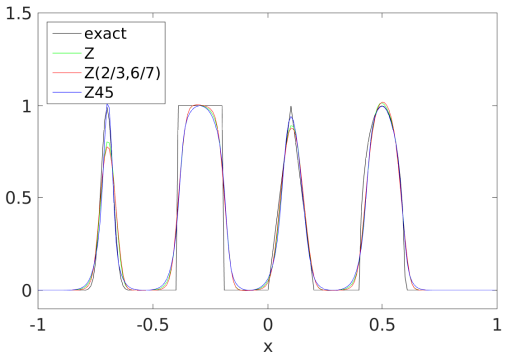

Figure 11a: Numerical solutions to the advection equation.

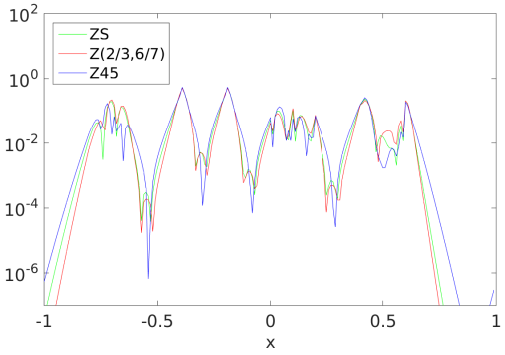

Figure 11b: Error compared to the exact solution.

Figure 11: Results for the linear advection equation using WENO-Z (green) and its embedded variants, WENO-Z45 (blue) and WENO-Z($\frac{2}{3},\frac{6}{7}$) (red). Solutions were computed on a periodic domain at $t = 8$, using 200 grid points and a CFL number of 0.45.

space between the shapes. The WENO-Z45 scheme captures the compact support of the shapes slightly worse than the standard scheme. However, it captures the maxima and minima better, which is due to the decreased dissipation inherent in the fourth-order inner scheme.

4.2. Shallow water equations

Finally, we consider the shallow water equations (SWE) for one-dimensional flow in a straight canal, i.e.,

$$\frac{\partial \psi}{\partial t} + \frac{\partial}{\partial x}(\psi u) = 0, \tag{61a}$$

$$\frac{\partial}{\partial t}(\psi u) + \frac{\partial}{\partial x}\left(\psi u^2 + \tfrac{1}{2}\psi^2\right) = 0, \tag{61b}$$

where u is the velocity and ψ is the geopotential. Introducing $\mathbf{u} = (u_1, u_2)^T$ with components $u_1 = \psi$ and $u_2 = u\psi$, we can write (61) as

$$\partial_t \mathbf{u} + \partial_x \mathbf{f}(\mathbf{u}) = 0. \tag{62}$$

After averaging over a cell $(x_{j-\frac{1}{2}}, x_{j+\frac{1}{2}})$, we obtain

$$\frac{\mathrm{d}}{\mathrm{d}t}\mathbf{u}_j + \frac{1}{\Delta x}\left(\mathbf{f}(\mathbf{u}_{j+\frac{1}{2}}) - \mathbf{f}(\mathbf{u}_{j-\frac{1}{2}})\right) = 0. \tag{63}$$

We employ the Godunov flux as our numerical flux function, i.e., we replace $\mathbf{f}(\mathbf{u}_{j+\frac{1}{2}})$ by $\mathbf{F}_G(\mathbf{u}^+_{j+\frac{1}{2}}, \mathbf{u}^-_{j+\frac{1}{2}})$, where $\mathbf{u}^\pm_{j+\frac{1}{2}}$ are the left and right-sided limits of the value of $\mathbf{u}$ on the cell edge. We then obtain the following semi-discretized scheme,

$$\frac{\mathrm{d}}{\mathrm{d}t}\mathbf{u}_j + \frac{1}{\Delta x}\left(\mathbf{F}_G(\mathbf{u}^+_{j+\frac{1}{2}}, \mathbf{u}^-_{j+\frac{1}{2}}) - \mathbf{F}_G(\mathbf{u}^+_{j-\frac{1}{2}}, \mathbf{u}^-_{j-\frac{1}{2}})\right) = 0. \tag{64}$$

The values for $\mathbf{u}$ on the cell edges are reconstructed by a WENO scheme. We then use the total variation diminishing Runge-Kutta time integrator from (16).

We consider two Riemann problems for the SWE, one subcritical dam break problem and one supercritical dam break problem. The initial condition for any Riemann problem is given by

$$(\psi_0, u_0)(x) = \begin{cases} (\psi_l, u_l) & \text{if } x < 0, \\ (\psi_r, u_r) & \text{if } x > 0. \end{cases} \tag{65}$$

Since the solution to the Riemann problem of the SWE is known, we can exactly calculate the global error, given by

$$e(\Delta x) := \sum_j |u_j^M - u(x_j, T)|\Delta x, \tag{66}$$

where $n = 1, \ldots, N$ and $T = M\Delta t$. However, we can also investigate more localized errors by letting n run only over the grid points within a certain interval $(x_{\text{left}}, x_{\text{right}})$. In this way, we can investigate the error behaviour in the rarefaction wave, intermediate state and the shock separately.

4.2.1. Subcritical dam break problem

The subcritical dam break problem has an initial condition given by

$$(\psi_l, u_l) = (\tfrac{7}{10}, 0), \quad (\psi_r, u_r) = (\tfrac{1}{10}, 0). \tag{67}$$

This leads to an intermediate state given by

$$(\psi^*, u^*) = (0.5512, 0.3148), \tag{68}$$

such that $\sqrt{\psi^*} > u^*$, meaning the flow in the intermediate state is subcritical. This solution produces a rarefaction wave on the left and a shock on the

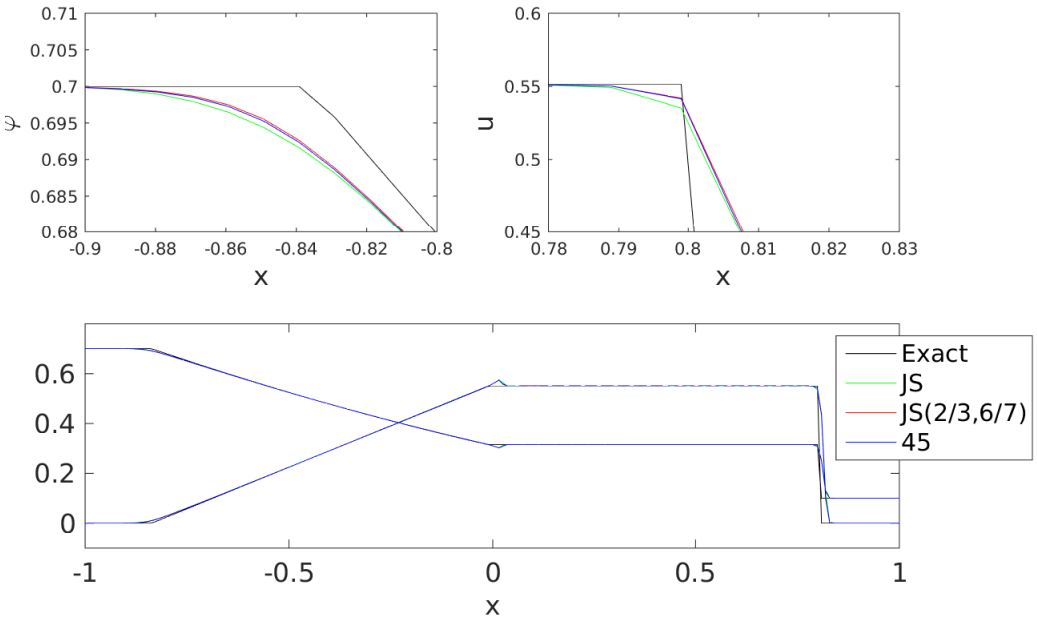

Figure 12: The numerical results for the WENO-JS based schemes for the subcritical dam break problem. We have used 200 grid points, a CFL number of 0.45 and $t = 1$.

right of the intermediate state. The result for WENO-JS and its embedded schemes are shown in Figure 12. The results of the standard scheme and the embedded variants are globally the same, producing a high resolution numerical solution. However, if we zoom in on the onset of the rarefaction wave and the shock, we see that locally, the embedded schemes give a smaller error.

We have computed the solution for several different grid sizes to obtain some information on the convergence of the scheme. The convergence around the shock will inherently be rather rough as a function of Δx, there might be large differences even by adding one more grid point. Thus, localising the error around the shock will not allow us to estimate the convergence behaviour. However, we can measure the effects of the shock by investigating the error in the intermediate state. Hence, we take $(x_{\text{left}}, x_{\text{right}}) = (0, 0.8)$, which is a large part of the intermediate state. The results are displayed in Table 4. It becomes clear that the embedded schemes give a smaller error and a slightly higher convergence rate. We can compute the average percentile increase in convergence rate, showing that WENO-JS$(\frac{2}{3}, \frac{6}{7})$ has a 11.29% increase and WENO-45 has a 10.28% increase in convergence rate,

as measured against WENO-JS.

Table 4: Error of the WENO-JS scheme and its embedded schemes over the intermediate state of the subcritical dam break problem. The orders are estimated by Richardson extrapolation.

N	$e_{\mathrm{JS}} \cdot 10^5$	order	$e_{\mathrm{JS}(\frac{2}{3},\frac{6}{7})} \cdot 10^5$	order	$e_{45} \cdot 10^5$	order
301	6.0685		5.6030		5.5939	
451	3.4451	0.8168	3.0570	0.8741	3.0409	0.8793
676	1.9811	0.7983	1.1714	0.8346	1.1768	0.8248
1014	1.0585	0.9043	0.8732	0.9732	0.8897	0.9483
1520	0.4991	1.0847	0.3386	1.3666	0.3468	1.3591

The same computation can be done for WENO-Z and its embedded variants, see Figure 13. The results are less spectacular than the previous results of the WENO-JS scheme. This is most likely due to the higher convergence rate of the WENO-Z nonlinear weights towards the linear weights, resulting in fifth-order accuracy in a greater part of the domain.

However, the results become much more telling if we switch time integrator to the Spiteri and Ruuth SSPRK(5,4) method. As mentioned in Section 1, the SSPRK(5,4) allows for a much larger CFL number, while still giving high-order accuracy. We therefore settle on a CFL number which is 2.5 times as large, $c = 1.125$. The embedded methods exhibit a much smaller error, capturing the onset of the rarefaction wave and the shock with much higher accuracy. At the same time, tests performed with WENO-JS schemes in tandem with SSPRK(5,4) hardly changes the error behaviour. It seems the error in the WENO-Z scheme is dominated by the time integrator while the error in the WENO-JS scheme is dominated by the spatial discretisation.

We can perform convergence tests for the combination of WENO-Z and its embedded variants together with SSPRK(5,4). The results are displayed in Table 5. The results show this time that order of convergence is roughly the same across all the variants. However, the embedded methods show an error which is roughly twice as small across the range. In fact, WENO-Z($\frac{2}{3}$, $\frac{6}{7}$) has an error which is on average 43.95% smaller, while WENO-Z45 has on average a 44.65% smaller error.

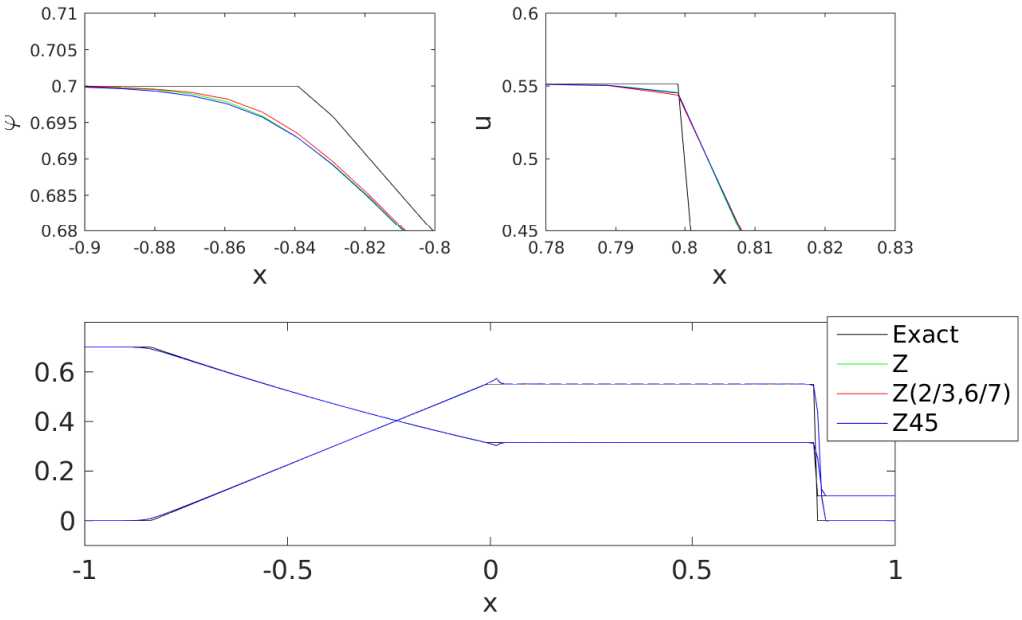

Figure 13: The numerical results for the WENO-Z based schemes for the subcritical dam break problem. We have used 200 grid points, a CFL number of 0.45 and $t = 1$.

4.2.2. Supercritical dam break problem

Finally, we will look at a supercritical dam break problem, where the initial condition is given by

$$(\psi_l, u_l) = (\tfrac{5}{2}, 0), \quad (\psi_r, u_r) = (\tfrac{1}{10}, 0). \tag{69}$$

This particular version of the dam break problem features supercritical flow in the intermediate region, since the intermediate state $(\psi^*, u^*) = (0.7158, 1.4701)$ is such that $u^* > \sqrt{\psi^*}$. Again, this solution features a rarefaction wave to the left of the intermediate state and a shock to the right. The result is shown in Figure 15.

Examining the figure, we can draw a similar conclusion to the subcritical case: globally, the schemes are roughly similar while locally, the embedded variants give a smaller error.

5. Conclusion

We have introduced a design method for WENO weights and with it a new family of WENO methods, which we have named the embedded

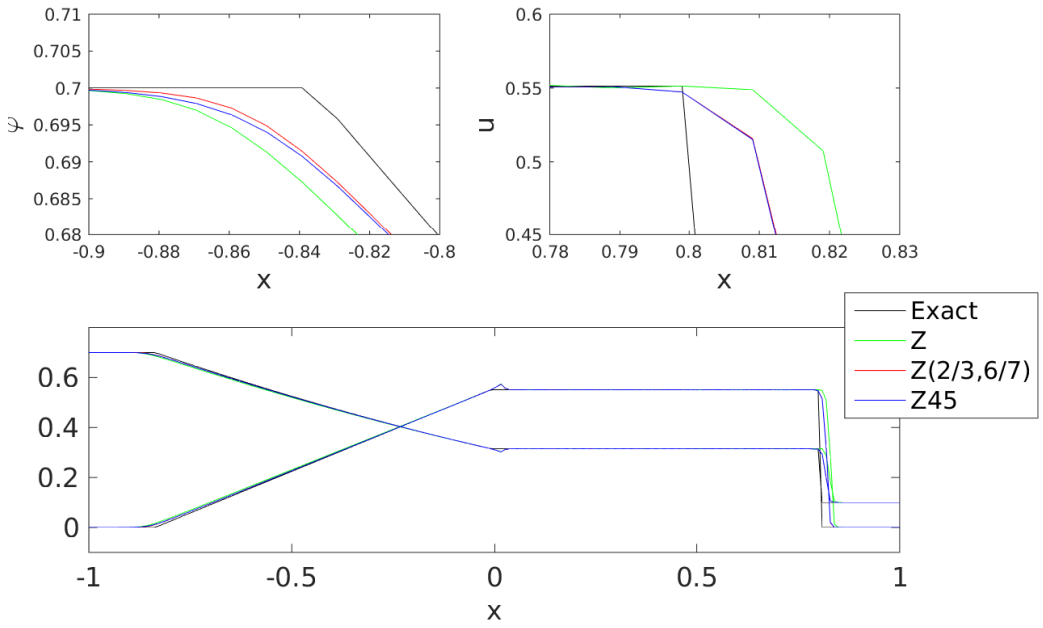

Figure 14: The numerical results for the WENO-Z based schemes for the subcritical dam break problem. We have used 200 grid points, a CFL number of 1.125 and $t = 1$. The time integration was performed by the SSPRK(5,4) integrator.

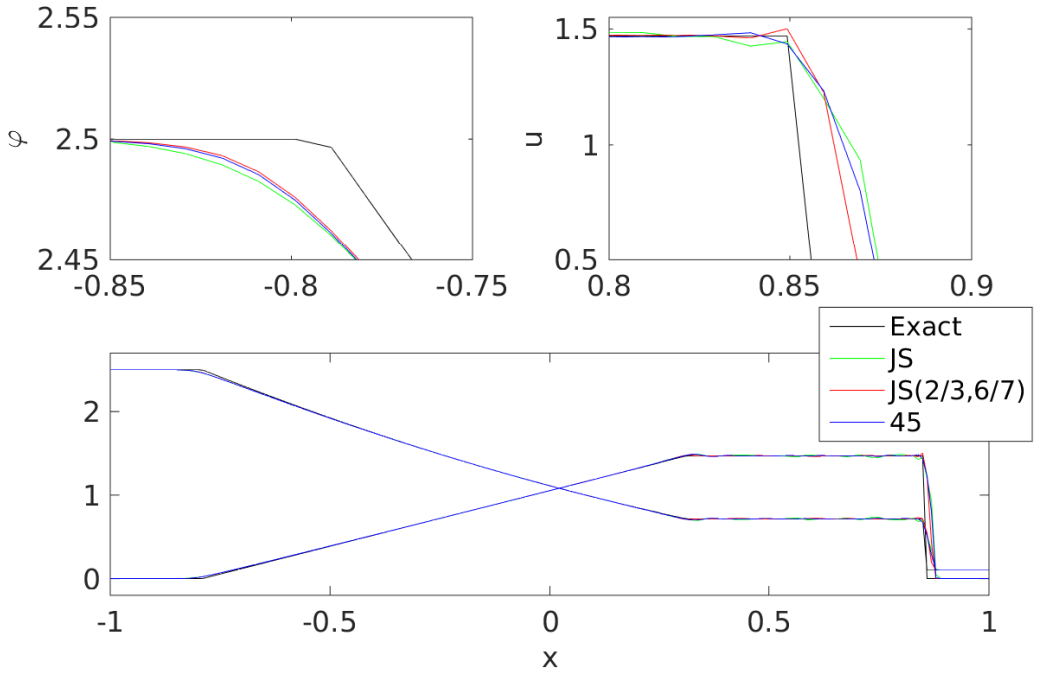

Figure 15: The numerical results for the WENO-JS based schemes for the supercritical dam break problem. We have used 200 grid points, a CFL number of 0.45 and $t = \frac{1}{2}$.

Table 5: Error of the WENO-Z scheme and its embedded schemes over the intermediate state of the subcritical dam break problem. Time integration was performed using SSPRK(5,4) and a CFL number of 1.125. The orders are estimated by Richardson extrapolation.

N	$e_{\mathrm{JS}} \cdot 10^4$	order	$e_{\mathrm{Z}(\frac{2}{3},\frac{6}{7})} \cdot 10^4$	order	$e_{45} \cdot 10^4$	order
301	4.0169		2.5810		2.5465	
451	2.1994	1.4855	1.4093	1.4924	1.3912	1.4910
676	0.8743	2.2751	0.4430	2.8540	0.4374	2.8539
1014	0.4776	1.4909	0.2418	1.4924	0.2387	1.4934
1520	0.2620	1.4812	0.1326	1.4829	0.1312	1.4765

WENO methods. The design method allows one to adapt the nonlinear weights of a particular WENO method. We named the overall third-and-fifth-order method the outer method, while the adjustment was dubbed the inner method. The inner method takes over when two adjacent substencils are smooth and the third one is not. In such regions, a conventional WENO method reverts to its third-order mode. This is slightly overzealous, as one has a four-point smooth stencil to work with. The embedded WENO schemes switch to their inner scheme in these cases. This allows more control over the numerical solution, for instance by attaining a higher order of convergence.

We have demonstrated through spectral analysis and several numerical experiments the benefits of the embedded WENO schemes over their corresponding standard methods. We have performed several numerical experiments which all show the same properties: equal or better performance in smooth regions and better performance near discontinuities in the solution and its derivative.

We have explicitly constructed embedded schemes based on the five-point WENO-JS and the WENO-Z method. However, as the design principles are general, we do not see great difficulties in making embedded versions of any given WENO method. The same principles can be applied to higher-order methods or any other type of WENO method.

Acknowledgements

This work was generously supported by Philips Lighting and the Intelligent Lighting Institute.

[1] G.-S. Jiang, C.-W. Shu, Efficient implementation of weighted ENO schemes, J. Comput. Phys. 126 (1996) 202 – 228.

[2] R. Borges, M. Carmona, B. Costa, W.-S. Don, An improved weighted essentially non-oscillatory scheme for hyperbolic conservation laws, J. Comput. Phys. 227 (2008) 3191 – 3211.

[3] A. Harten, S. Osher, Uniformly high-order accurate nonoscillatory schemes. I, SIAM J. Numer. Anal. 24 (2) (1987) 279–309.

[4] X.-D. Liu, S. Osher, T. Chan, Weighted essentially non-oscillatory schemes, J. Comput. Phys. 115 (1) (1994) 200 – 212.

[5] T. J. Barth, H. Deconinck (Eds.), High-Order Methods for Computational Physics, Springer, 1999, Ch. High order ENO and WENO schemes for computational fluid dynamics by C.W. Shu, pp. 439 – 582.

[6] J.-M. Qiu, C.-W. Shu, L.-L. Feng, L.-Z. Fang, A WENO algorithm for the radiative transfer and ionized sphere at reionization, New Astronomy 12 (1) (2006) 1–10.

[7] S. Amat, S. Busquier, J. C. Trillo, On multiresolution schemes using a stencil selection prodecure: Applications to ENO schemes, Numer. Algorithms 44 (2007) 45 – 68.

[8] K. Siddiqi, B. B. Kimia, C.-W. Shu, Geometric shock-capturing ENO schemes for subpixel interpolation, computation and curve evolution, Graphical Models and Image Processing 59 (1997) 278 – 301.

[9] A. K. Henrick, T. D. Aslam, J. M. Powers, Mapped weighted essentially non-oscillatory schemes: achieving optimal order near critical points, J. Comput. Phys. 207 (2005) 542 – 567.

[10] H. Feng, F. Hu, R. Wang, A new mapped weighted essentially non-oscillatory scheme, J. Sci. Comput. 51 (2) (2012) 449 – 473.

[11] M. Castro, B. Costa, W. S. Don, High order weighted essentially non-oscillatory WENO-Z schemes for hyperbolic conservation laws, J. Comput. Phys. 230 (5) (2011) 1766 – 1792.

[12] F. Aràndiga, M. Martí, P. Mulet, Weights design for maximal order WENO schemes, J. Sci. Comput. 60 (2014) 641 – 659.

[13] Y. Ha, C. H. Kim, Y. J. Lee, Y. Yoon, An improved weighted essentially non-oscillatory scheme with a new smoothness indicator, J. Comput. Phys. 232 (1) (2013) 68 – 86.

[14] S. Zhao, N. Nardjane, I. Fedioun, Comparison of improved finite-difference WENO schemes for the implicit large eddy simulation of turbulent non-reacting and reacting high-speed shear flows, Computers & Fluids 95 (2014) 74 – 87.

[15] N. K. Yamaleev, M. H. Carpenter, Third-order energy stable WENO scheme, J. Comput. Phys. 228 (8) (2009) 3025 – 3047.

[16] N. K. Yamaleev, M. H. Carpenter, A systematic methodology for constructing high-order energy stable WENO schemes, J. Comput. Phys. 228 (11) (2009) 4248 – 4272.

[17] F. Jia, Z. Gao, W. S. Don, A spectral study on the dissipation and dispersion of the WENO schemes, J. Sci. Comput. 63 (1) (2015) 49 – 77.

[18] M. P. Martin, E. M. Taylor, M. Wu, V. G. Weirs, A bandwidth-optimized WENO scheme for the effective direct numerical simulation of compressible turbulence, J. Comput. Phys. 220 (1) (2005) 270 – 289.

[19] P. Fan, Y. Shen, B. Tian, C. Yang, A new smoothness indicator for improving the weighted essentially non-oscillatory scheme, J. Comput. Phys. 269 (2014) 329 – 354.

[20] S. Zhang, C.-W. Shu, A new smoothness indicator for the WENO schemes and its effect on the convergence to steady state solutions, J. Sci. Comput. 31 (2007) 273 – 305.

[21] S. Gottlieb, C.-W. Shu, Total variation diminishing Runge-Kutta schemes, Mathematics of Compuation 67 (221) (1998) 73 – 85.

[22] S. Gottlieb, C.-W. Shu, E. Tadmor, Strong stability-preserving high-order time discretization methods, SIAM Review 43 (1) (2001) 89 – 112.

[23] R. Wang, R. J. Spiteri, Linear instability of the fifth-order WENO method, SIAM J. Numer. Anal. 45 (5) (2007) 1871 – 1901.

[24] R. J. Spiteri, S. J. Ruuth, A new class of optimal high-order strong-stability-preserving time discretization methods, SIAM J. Numer. Anal. 40 (2) (2002) 469 – 491.

PREVIOUS PUBLICATIONS IN THIS SERIES:

Number	Author(s)	Title	Month
15-25	M.H. Duong A. Lamacz M.A. Peletier U. Sharma	Variational approach to coarse-graining of generalized gradient flows	July '15
15-26	E.N.M. Cirillo M. Colangeli A. Muntean	Effects of communication efficiency and exit capacity on fundamental diagrams for pedestrian motion in an obscure tunnel – a particle system approach	July '15
15-27	S. Karpinksi I.S. Pop	Analysis of an interior penalty discontinuous Galerkin scheme for two phase flow in porous media with dynamic capillarity effects	July '15
15-28	J.H.M. Evers S.C. Hille A. Muntean	Measure-valued mass evolution problems with flux boundary conditions and solution-dependent velocities	July '15
15-29	B.S. van Lith J.H.M. ten Thije Boonkkamp W.L. IJzerman	Embedded WENO: a design method to improve existing WENO schemes	July '15

Ontwerp: de Tantes,
Tobias Baanders, CWI